# Electron Hopping through TiO2 Powder: A Study by Photoluminescence Spectroscopy

**ARTICLE** *in* THE JOURNAL OF PHYSICAL CHEMISTRY C · NOVEMBER 2013

Impact Factor: 4.77 · DOI: 10.1021/jp407765r



**2 AUTHORS**, INCLUDING:

Ana Stevanovic
National Institute of Standards and Technology
**7** PUBLICATIONS **52** CITATIONS

SEE PROFILE

THE JOURNAL OF PHYSICAL CHEMISTRY C

Article

pubs.acs.org/JPCC

# Electron Hopping through $TiO_2$ Powder: A Study by Photoluminescence Spectroscopy

Ana Stevanovic and John T. Yates, Jr.*

Department of Chemistry University of Virginia, Charlottesville, Virginia 22904, United States

**ABSTRACT:** Photoluminescence spectroscopy was employed to observe electron transport between $TiO_2$ particles. Ultraviolet (UV) irradiation (3.88 eV) was shown to positively enhance the photovoltage of $TiO_2$ particles at the powder surface, causing an enhancement of their photoluminescence (PL) at 530 nm. The charging of the $TiO_2$ particles on the powder surface by UV irradiation partially discharges in the dark, where the displaced bulk negative charge diffuses back toward the $TiO_2$ surface. This charge flow partially restores upward band bending, causing the PL intensity to decrease. The rate of the discharging process was used to estimate the electron migration mobility ($\sim 10^{-10}$ $m^2$ $V^{-1}$ $s^{-1}$ at 300 K) between $TiO_2$ particles in the $TiO_2$ matrix. Electron migration between $TiO_2$ particles is temperature-dependent with an activation energy of 0.015 ± 0.008 eV. In addition, it was found that the adsorption of an immobile electron-donor molecule ($NH_3$), attracts negative charge on the $TiO_2$ surface which does not exhibit mobility behavior, in contrast to mobile electrons produced by UV. These measurements were carried out in high vacuum in the absence of oxygen and surface impurities detectable by IR spectroscopy.

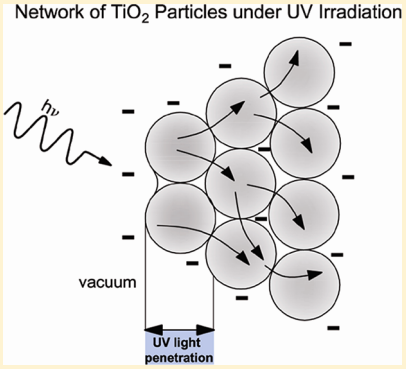


## 1. INTRODUCTION

Nanostructures of metal oxides such as $TiO_2$, ZnO, $SnO_2$, and $Nb_2O_5$ have attracted great attention in photovoltaic applications because of their ability to capture and convert sunlight into electrical energy.[1−4] Among these metal oxides, the most intensively studied material is the n-type $TiO_2$ semiconductor because of its superior properties, which are heavily utilized for photovoltaic purposes[5,6] and in photocatalysis.[7−10] In $TiO_2$-based photovoltaic devices, the semiconductor particles are sensitized with a light-harvesting dye molecule that serves to deliver photogenerated electrons into a network of interconnected $TiO_2$ particles. The electrons percolate among interconnected $TiO_2$ particles and are collected by an electrode. In mesoporous $TiO_2$, electrons in single crystallites travel by crossing several particle−particle interfaces. In $TiO_2$ involving 20-nm-sized particles, electrons can cross as many as 50 interfaces in a typical photovoltaic cell.[11−13] It was shown that the photoconductivity of the mesoporous $TiO_2$ single-crystal material is 2 orders of magnitude higher than the photoconductivity in a nanometer $TiO_2$ particle network because of the lower number of particle−particle interfaces. An understanding of charge transport in networks of semiconductor particles is essential for improving the efficiency of photovoltaic devices involving porous semiconducting materials.

Charge transport has been intensively studied by optical and electrical methods such as photovoltage measurements,[14,15] impedance spectroscopy,[16] Hall effect measurements,[17,18] photoluminescence,[19] and also modeling.[20−22] Electron transport in porous $TiO_2$ occurs under UV exposure, as shown by Dittrich and co-workers[14] and others,[23,24] as photogenerated electrons in the conduction band move either freely or by trapping−detrapping processes from particle to particle across the $TiO_2$ network. Using tetrahertz time-domain spectroscopy, it was found that the average charge mobility within a $TiO_2$ nanoparticle is 4 orders of magnitude larger[25] than the charge mobility between $TiO_2$ particles in a $TiO_2$ matrix that does not contain electrolyte.[26,27] In an electrolyte-filled $TiO_2$ matrix, electron mobility between $TiO_2$ particles is about an order of magnitude faster than that in a porous $TiO_2$ network.[28,29]

The surface and electronic properties of porous $TiO_2$ depend strongly on the presence of adsorbed molecules on the surface, as adsorbates perturb the distribution of electron trap sites, thus affecting electron conductivity. The vast majority of reports on charge-carrier transport in porous materials present measurements performed in air or in different solutions where the surface electronic properties of $TiO_2$ are altered from those found in vacuum. For example, it was found that in porous nanocrystalline $TiO_2$, the conductivity of charge carriers in $TiO_2$ particles increases by 6 orders of magnitude under vacuum conditions due to the removal of adsorbed oxygen.[23] It is postulated that lattice oxygen removal by annealing leads to excess electrons in the surface-oxygen vacancy defect sites. The excess electrons contribute to increased conductivity[30] and to upward band bending.[31] Compared to measurements in air, the experiments presented in this work involve a high level of control of the surface, as the $TiO_2$ preparation and measurements are conducted under high-vacuum conditions and species adsorbed on the surface are monitored by IR spectroscopy.

**Received:** August 3, 2013
**Revised:** October 17, 2013
**Published:** October 17, 2013

   dx.doi.org/10.1021/jp407765r | J. Phys. Chem. C 2013, 117, 24189−24195

In $TiO_2$ powder, in the case of n-type material, the production of electron−hole pairs occurs only in the very outer surface region of the powder because of the short penetration depth (∼20 nm) of the exciting UV irradiation.[32−35] The UV Irradiation causes the development of a positive surface photovoltage that is confined to the outermost $TiO_2$ particles in the powder where the particle size is of the same order of magnitude as the light penetration depth. The $TiO_2$ surface is oxygen-deficient and, therefore, n-type because of the excess electrons in the lattice-oxygen vacancies on the surface, which increase the electronic potential energy near the surface, causing the bands to bend upward. Here, under UV irradiation, energetically preferred electron transport occurs into the bulk from the surface of the particles where the bands are initially bent upward.[36−38] In this region, electron−hole ($e^-$−$h^+$) recombination is retarded as charges are swept away from each other due to the electric field in the first 10−20 nm of the $TiO_2$ surface. UV irradiation therefore decreases the depletion layer thickness. The positive charge accumulation at the $TiO_2$ surface during UV irradiation lowers the surface electrostatic potential, causing initially upward-bent bands to flatten. As a result, UV irradiation causes the photoluminescence intensity to be enhanced[31,32,39−41] as more semiconductor volume within the UV-light penetration depth becomes available for $e^-$−$h^+$ recombination.

In this investigation, using photoluminescence (PL) spectroscopy, we observed, under high-vacuum conditions, the change in surface photovoltage upon UV irradiation of interconnected $TiO_2$ particles. Here, surface negative charge is distributed into the bulk by absorption of energetic photons (3.88 eV) (Figure 1A). Our key finding is that, upon discontinuation of UV irradiation, some of the negative charge originally distributed in the $TiO_2$ network returns to the surface of the outermost $TiO_2$ particle (Figure 1B), partially restoring the upward band bending and reducing the PL intensity. Here, the production of a charged powdered $TiO_2$ surface by UV irradiation, followed by its discharge in the dark by migration of displaced electrons back to the surface, can be viewed as the behavior of a planar capacitor. The rate of discharge can be used to estimate the charge mobility as electrons hop from particle to particle if the electric field inducing electron mobility can be estimated. In addition, it was found that this process is temperature-dependent as the rate of electron hopping between particles is enhanced at higher temperatures. Further, we have employed a chemical species, an electron-donor molecule ($NH_3$), to produce immobilized positively charged species on the $TiO_2$ surface analogous to the surface charging during irradiation. As expected, upon discontinuation of UV irradiation when adsorbed $NH_3$ is present, electrons in $TiO_2$ do not transport in the same manner as observed for electrons when the surface is positively charged by UV photons.

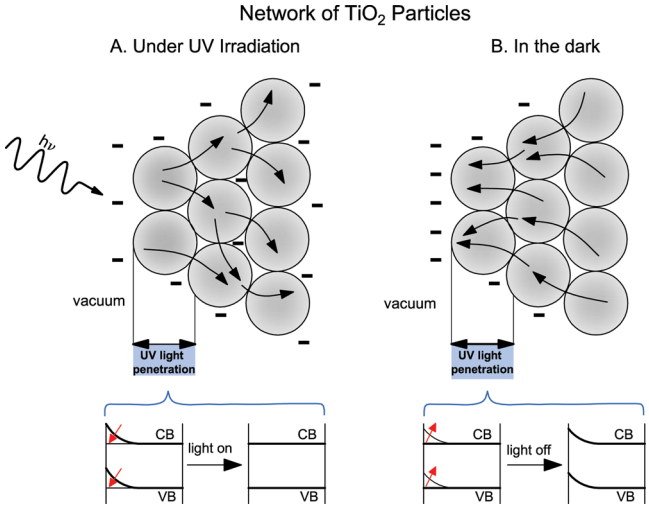


**Figure 1.** (A) Distribution of surface negative charge into the $TiO_2$ powder caused by absorption of UV photons and inducing a more positive surface photovoltage on the outer $TiO_2$ particles, causing band flattening. (B) Diffusion of the bulk negative charge back to the $TiO_2$ surface in the dark, partially restoring upward band bending.

## 2. EXPERIMENTAL SECTION

The experimental apparatus was described previously.[32] In brief, a stainless steel optical cell with $CaF_2$ windows was employed, allowing both PL and transmission IR measurements to be made on powdered $TiO_2$. The base pressure in the high-vacuum stainless steel cell after bakeout was $\sim 3.0 \times 10^{-9}$ Torr as measured by a cold cathode gauge or a quadrupole mass spectrometer (SRS model RGA 200). The $TiO_2$ powder sample was fabricated as a pressed disk held in a temperature-controlled tungsten grid. The high-vacuum cell was rigidly attached to a small portable high-vacuum system, allowing it to be moved under high vacuum from an infrared spectrometer (Perkin-Elmer Spectrum 100) to an adjacent photoluminescence spectrometer (Perkin-Elmer LS-55), maintaining the cell position accurately constant in both spectrometers. The $TiO_2$ powder was pressed with 6000 psi into a 0.0095-cm-thick tungsten grid, filling hundreds of window openings ($0.022 \times 0.022$ $cm^2$) by the creation of a 7-mm-diameter circular spot that could be accurately positioned in the UV or IR optical beam. The mass of the $TiO_2$ sample was $5.9 \times 10^{-3}$ g. The sample was held on a tungsten grid that was clamped to a Cu (OFHC) sample holder that was connected to electrical feedthroughs and mounted on the end of a re-entrant Dewar. The temperature of the sample was measured by a 0.0076-cm-diameter K-type thermocouple, spot-welded on the center top of the grid. Temperature control to 0.1 K was achieved using liquid-$N_2$ cooling and electrical heating. The temperature of the grid could be linearly programmed between 84 and 1000 K by using a data acquisition card (National Instrument, DAC) and feedback from the thermocouple to control the heating current. This allowed for precise isothermal measurements.

The photoluminescence measurements employed 320 ± 10 nm (3.88 eV) incident light from a pulsed Xe source (60 Hz with a pulse width of <10 $\mu$s). The continuous power measured at the sample position was $9.1 \times 10^{-5}$ J $s^{-1}$ $cm^{-2}$ [$1.5 \times 10^{14}$ photons $cm^{-2}$ $s^{-1}$]. A grating and a 320-nm band-pass filter were employed on the source side. The spectra were obtained using a 15-nm slit width at the excitation side and a 20-nm slit width at the emission side with a scan speed of 500 nm $min^{-1}$. The PL spectra were detected by an R928 photomultiplier tube covering the 200−900-nm range. For the PL measurements, the sample is positioned 15° off the specular reflection direction of the source light to minimize detection of the reflected incident light from the sample surface and from the $CaF_2$ window.

The $TiO_2$ powdered samples employed in this work were provided by Evonik Industries (P-25, formerly Degussa). The P-25 $TiO_2$ consists of 75% of anatase and 25% rutile phase with particle sizes between 30 and 80 nm and a surface area[50] of 50


dx.doi.org/10.1021/jp407765r | J. Phys. Chem. C 2013, 117, 24189−24195

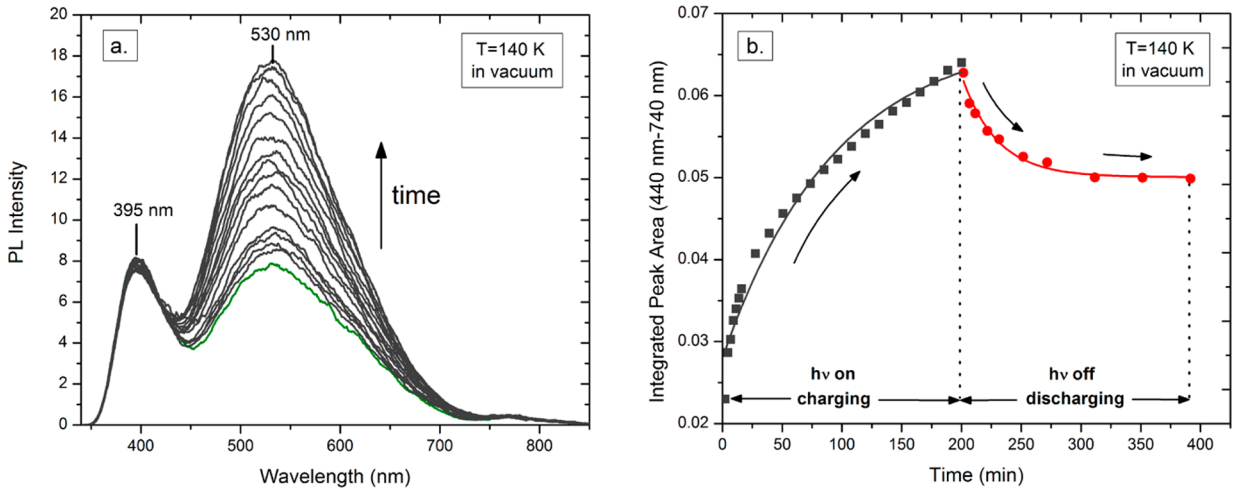


**Figure 2.** (a) Development of a 530-nm $TiO_2$ photoluminescence feature during continuous UV irradiation in vacuum at 140 K. (b) Change in PL intensity during and upon discontinuation of UV irradiation in vacuum at 140 K. Black curve shows an exponential increase in PL intensity upon irradiation of $TiO_2$ particles indicating a decrease in the surface negative charge due to electron hopping then occurs from particle to particle, negatively charging the interior of the $TiO_2$ network. The red curve shows a decrease in the PL intensity of the $TiO_2$ particles as negative charge transports from the interior of the $TiO_2$ powder back to the surface, partially restoring upward band bending.

$m^2\ g^{-1}$. A water slurry of $TiO_2$ particles was dried in air at 353 K. Additional adsorbed water was removed by treatment of the pressed sample in vacuum at 650 K for 30 min. Further thermal treatment at 650 K in vacuum followed by treatment in $O_2$(g) at 0.5 Torr for 30 min at 650 K was carried out. The sample was finally treated in vacuum at 650 K for 10 min and then cooled to liquid-nitrogen temperatures in vacuum for the experiments. Following this treatment, the IR spectrum of the sample indicated that no OH- and C−H-containing adsorbed species were present at the detection limit of about 1% of a monolayer. The oxygen treatment was shown to effectively remove traces of adsorbed organic impurities that display C−H stretching modes in the 3000 $cm^{-1}$ region.

## 3. EXPERIMENTAL RESULTS

**3.1. Charging and Discharging of the $TiO_2$ Surface.** In Figure 2a, the black spectra with maxima at 530 nm show that the PL intensity from $TiO_2$ particles increases during long UV exposures using the light in the PL spectrometer to activate long-term changes in the $TiO_2$. The peak at 395 nm is an optical artifact and is disregarded.[32] In Figure 2b, black points show the development of the 530-nm peak over time. The PL intensity ultimately approaches a near-saturation plateau indicating a near-flat-band condition. Here, the concentration of negative surface charge diminishes as electrons are distributed into the network of $TiO_2$ particles (charging process), as shown in Figure 1A. In Figure 2b, the red curve shows that the PL intensity decreases upon discontinuation of UV irradiation for 192 min in vacuum (discharging process), as shown in Figure 1B. The PL intensity reaches its minimum value when only a fraction of distributed electrons diffuse from the depth of the powder back to the surface, thereby causing only partial restoration of upward band bending of the outermost particles. These measurements in the dark involve short UV exposures of 45 s each, yielding a measurement of the discharging rate as seen by the drop in the PL intensity, where the long-term influence of the UV light can be disregarded as it is only 2.5% of that used to produce the initial charging curve.

**3.2. Electron Migration from Particle to Particle.** Figure 3 shows several consecutive charging/discharging cycles of the

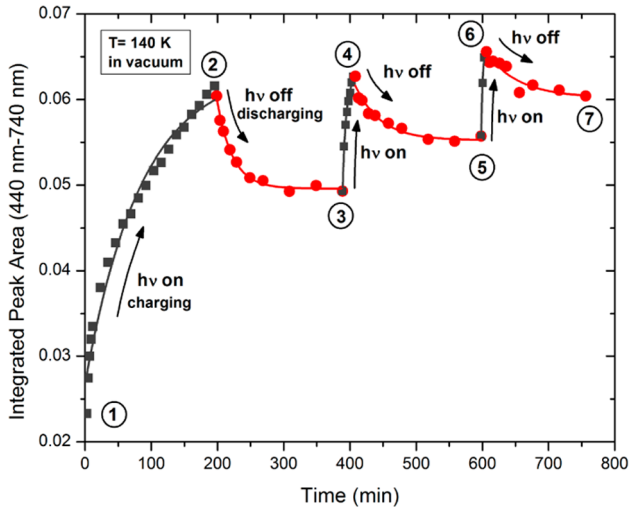


**Figure 3.** Photoluminescence development upon UV irradiation (gray squares) and relaxation in the dark (red circles) at 140 K in vacuum. During the three UV irradiation cycles (shown by gray squares), the rate of photoluminescence intensity increase yields the slowest development in the first cycle ($k_{1-2}$ = 2 × $10^{-4}$ $s^{-1}$) and faster development during the second and third irradiation cycles ($k_{3-4}$ = 3 × $10^{-4}$ $s^{-1}$ and $k_{5-6}$ = 3 × $10^{-3}$ $s^{-1}$, respectively). Upon interruption of UV light (shown by red circles), the rate of change of the PL intensity decreases as time passes, giving PL decay rates of $k_{2-3}$ = 7 × $10^{-4}$ $s^{-1}$, $k_{4-5}$ = 4 × $10^{-4}$ $s^{-1}$, and $k_{6-7}$ = 3 × $10^{-4}$ $s^{-1}$.

$TiO_2$ network at 140 K in vacuum. During the UV irradiation cycles, the PL intensity increases (shown by the black curves) as negative surface charge diffuses deeper into the network of $TiO_2$ particles, leaving less charge on the surface and causing upward-bent bands to flatten (point 2). As previously discussed, the bands flatten as UV light causes electrons to leave the surface of the $TiO_2$ particles located on the outermost surface of the powder. Upon discontinuation of UV irradiation (shown by the red curve), partial relaxation occurs as the PL intensity exponentially decreases as electrons diffuse back from the bulk onto the $TiO_2$ surface. The rate of charge diffusion from the surface into the $TiO_2$ powder bed by UV irradiation increases


dx.doi.org/10.1021/jp407765r | J. Phys. Chem. C 2013, 117, 24189−24195

as higher levels of PL intensity are produced in successive experiments (black curves) with rate constants of $k_{1-2} = 2 \times 10^{-4}$ s$^{-1}$, $k_{3-4} = 3 \times 10^{-4}$ s$^{-1}$, and $k_{5-6} = 3 \times 10^{-3}$ s$^{-1}$. On the other hand, the rate of charge diffusion from the bulk to the surface of the $TiO_2$ network in the dark in vacuum, decreases as time passes, with discharge time rates of $k_{2-3} = 7 \times 10^{-4}$ s$^{-1}$, $k_{4-5} = 4 \times 10^{-4}$ s$^{-1}$, and $k_{6-7} = 3 \times 10^{-4}$ s$^{-1}$. The reason for the decreasing rate of discharge is that, during the passage of time in the experiment, electronic charge penetrates more and more deeply into the bulk and becomes unavailable for back-diffusion.

**3.3. Adsorbed $NH_3$: Immobilization of Surface Charge in Interconnected $TiO_2$ Particles.** We studied the adsorption of the electron-donor molecule $NH_3$ onto $TiO_2$ particles to determine whether the deposition of an immobile charged chemical species would show different behavior from the displacement of mobile electrons. Adsorption of $NH_3$ was performed at 120 K, which is a temperature at which electrons are mobile in $TiO_2$. In Figure 4, the green point shows the PL intensity from a clean n-type $TiO_2$ surface in vacuum at 120 K, which represents an initial upward band-bending condition of the n-type material. Upon admission of $\sim 8 \times 10^{16}$ $NH_3$ molecules in the dark, the PL intensity initially rises as a result of the flattening of the band. Chemisorbed $NH_3$ causes the partial cancellation of the local negative-outward surface dipole on the outer $TiO_2$ n-type particle (as shown by the red points). Following $NH_3$ adsorption in the dark at 120 K, the PL intensity remains constant in vacuum for 130 min, which implies the presence of a stable surface charge on the $TiO_2$ particles in the outermost surface.

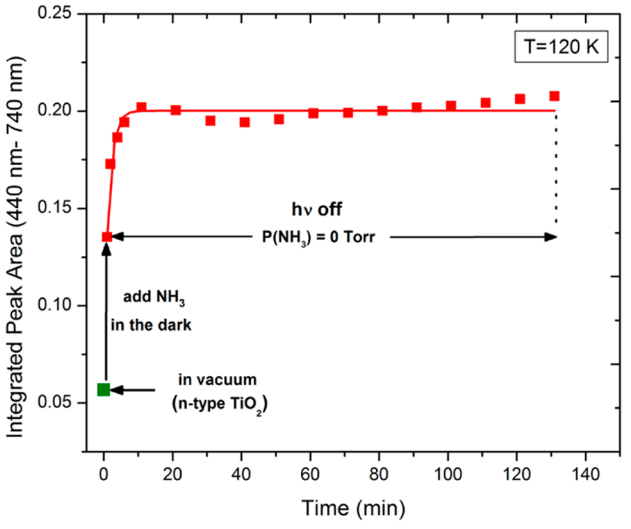


**Figure 4.** Immobilization of charges by chemical means. Adsorption of $NH_3$ on n-type $TiO_2$ surface with upward-bent bands at 120 K in the dark. Upon admission of $\sim 8 \times 10^{16}$ molecules of $NH_3$ (electron donor molecule), the PL intensity increases quickly as the upward-bent bands of $TiO_2$ flatten and the PL intensity then remains invariant over time in the dark.

This experiment strikingly demonstrates the contrasting behavior of mobile electrons as they hop between $TiO_2$ particles and immobile electrons as they remain attracted by positively charged adsorbate molecules that do not move into the interior of the $TiO_2$ powder at the temperature employed.[36] The sign of the behavior of the PL intensity and the rate of PL intensity change are measures of the mobility, and the direction of motion of electrons contrasted to the immobility of electrons upon adsorption of positively charged molecules.

**3.4. Temperature Dependence of Charge Migration between $TiO_2$ Particles.** In Figure 5, the black points show the normalized PL development under UV irradiation for ~184 min in vacuum. Here, the irradiated surface was initially brought to a near-flat-band condition. At 184 min, the UV light was blocked for 120 min at different temperatures, namely, 84, 100, 110, and 140 K. In the dark, the PL intensity exponentially decreases, and the rate of the discharging process increases, with rate constants of $k_{84\ K} = 1.9 \times 10^{-4}$ s$^{-1}$, $k_{100\ K} = 3.5 \times 10^{-4}$ s$^{-1}$, $k_{110\ K} = 3.9 \times 10^{-4}$ s$^{-1}$, and $k_{140\ K} = 4.6 \times 10^{-4}$ s$^{-1}$ as the temperature is increased from 84 to 140 K. Comparing data at all four temperatures, one sees that the rate of charge migration from the $TiO_2$ interior to the surface is reduced at lower temperatures, as judged by the rate of decay of the PL intensity in vacuum in the dark. Panel b shows the natural logarithm of the rate of charge migration between particles as a function of $T^{-1}$. Here, the error bars represent a ± 20% estimated error of the charge migration rate. The activation energy for the electron-transfer process determined from the plot is $E_a = 0.015 \pm 0.008$ eV.

## 4. DISCUSSION

**4.1. Diffusion of Electrons in $TiO_2$ Powder.** The planar powdered $TiO_2$ sample was pressed into rectangular units with dimensions of 0.022 cm × 0.022 cm × 0.0095 cm thickness inside a planar tungsten grid. Each small unit is a rectangular block of semiconducting powder with a back and front face exposed to vacuum and with the four edges connecting to tungsten oxide-coated-W boundaries. This corresponds to a material suspended with vacuum interfaces on the front and back and with insulating interfaces at the four edges. The tungsten grid holding the $TiO_2$ can be considered as an insulating support because of its thick oxide coating.[42] The geometry of each of the $TiO_2$ units is that of a suspended rectangular-shaped powder matrix without external contact, and it can therefore be considered as an isolated unit in vacuum.

UV light, incident on the front surface of the powdered matrix and mainly absorbed by the outermost $TiO_2$ particles, causes electron transport into the interior, producing a positive surface photovoltage (Figure 1) that serves to flatten the upward-bent bands of the outermost particles. This is associated with a PL intensity increase [exponential with time and UV flux ($F_{h\nu}$)] during long UV light exposures[32] in vacuum, as shown in Figure 2. When the light is turned off, the flattened bands start bending upward again, as negative charge inside the $TiO_2$ powder senses the more "positively" charged surface, and electrons return by slow hopping back to the surface. Because of the slow electron hopping throughout the powder matrix, the rate constant of decay in Figure 3 of the photovoltage in the dark is low and on the order of $4 \times 10^{-4}$ s$^{-1}$ at 140 K. The slow hopping of trapped electrons during discharging in the dark in anatase $TiO_2$ powder was also observed by both electron paramagnetic resonance (EPR) spectroscopy[43,44] and diffuse reflectance Fourier transform infrared (DRIFT-IR) spectroscopy[45] under high-vacuum conditions. This rate constant yields an electron mobility that is 7 orders of magnitude smaller than the electron mobility associated with in situ electron-transport processes in $TiO_2$ single crystals[25] and must therefore correspond to charge redistribution due to electron hopping over the surface of the $TiO_2$ particles and/or between $TiO_2$ particles. The electron


dx.doi.org/10.1021/jp407765r | J. Phys. Chem. C 2013, 117, 24189−24195

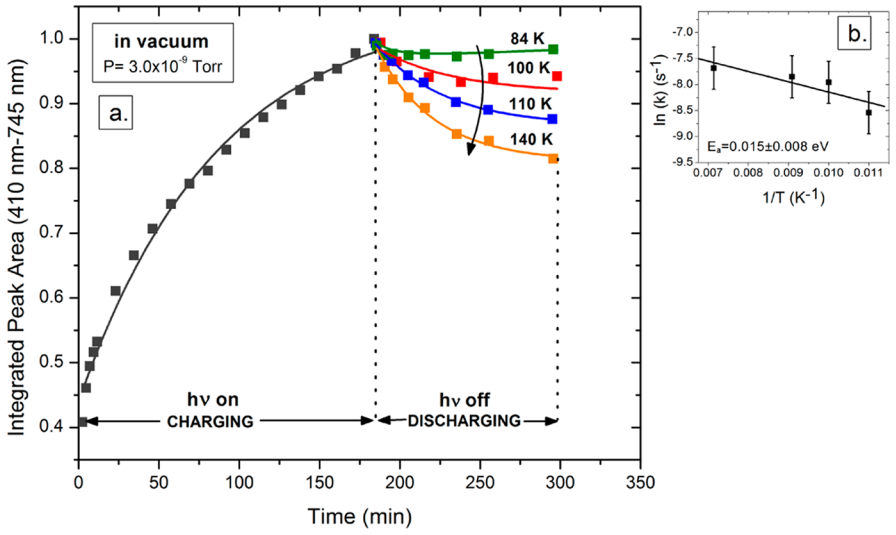


**Figure 5.** (a) Photoluminescence decay in the dark in vacuum at different temperatures. Black points represent the PL development upon UV irradiation. The $TiO_2$ surface was prepared to a near-flat band condition, as a saturation PL intensity plateau was almost achieved. Upon interruption of UV light, a PL decrease was observed at different temperatures: 84 K (green), 100 K (red), 110 K (blue), and 140 K (orange). (b) Natural logarithm of the rate of charge migration in the dark as a function of temperature where the extracted activation energy is 0.015 ± 0.008 eV. The data are normalized at the maximum PL intensity.

transport to the interior particles of the powdered matrix when UV light is on is accompanied by back-diffusion of charge to the surface. Hence, the measured rate of change in the PL intensity is the sum of the rate of forward diffusion, driven by UV light, and the rate of back-diffusion of electrons. When UV light is off, the observed PL behavior is directly related only to back-diffusion of electrons from the interior of the $TiO_2$ matrix back to the outermost $TiO_2$ particles, which then experience upward band bending and an associated reduction of PL intensity. Here, only a fraction of the bulk electrons migrates to the $TiO_2$ surface, as judged by the 20% reduction in PL intensity at 140 K, as most of the electrons are distributed deeper in the powder, where long hopping distances reduce electron back-diffusion rates to the surface. Most importantly, in the cyclical experiment of Figure 3, electrons are constantly diffusing into the interior as time passes. Figure 6 schematically shows the distribution of electron density, $n_e$, as time passes and electrons penetrate by diffusion deeper and deeper into the porous $TiO_2$ particle bed. The inward electron diffusion rate decreases as the gradient of electron density decreases with time. A back-diffusion rate component also exists in this picture, and as time

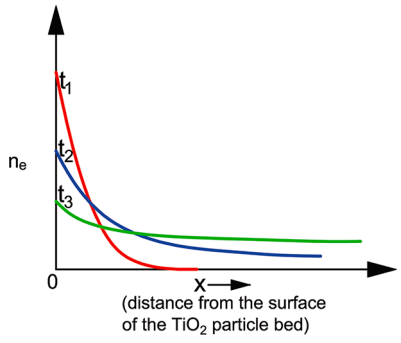


**Figure 6.** Diffusion of electrons over time in a $TiO_2$ network. The density of electrons ($n_e$) at the surface decreases as electrons diffuse deeper into the $TiO_2$ matrix. As time passes ($t_3 > t_2 > t_1$), more electrons are distributed into the $TiO_2$ matrix, as shown.

passes, despite the gradient behavior, the back-diffusion rate component will also decrease as electron density spreads to the interior as a result of the longer diffusion paths involved. Because the net rate of electron transport is the sum of the forward and backward component rates, as time passes for charging experiments with the UV irradiation on, the rate of charging (and hence the rate of increase in the PL intensity) will increase, reflecting the decrease in the back-diffusion rate for electrons that have penetrated more deeply into the $TiO_2$ matrix. Thus, in Figure 3, $k_{5-6} > k_{3-4} > k_{1-2}$. Conversely, as time passes and deeper electron penetration occurs, where the electron path length for back-diffusion increases, the rate of back-diffusion in Figure 3 will decrease and $k_{2-3} > k_{4-5} > k_{6-7}$. The rate component of back-diffusion is a convolution of the electron density gradient and the distances of electron diffusion to reach the surface at $x = 0$.

The behavior of mobile electrons is not observed when immobile adsorbate is used to produce surface charging. Thus, in Figure 4, the adsorption of $NH_3$, a donor molecule causing band flattening, is comparable to the production of a positive photovoltage and causes an enhancement of the PL intensity. However, because $NH_3$ is immobile at 120 K and does not diffuse or desorb away from the surface of the outermost $TiO_2$ particle,[36] the PL decay effect is not observed since "charge" mobility is absent due to the attraction of immobile $NH_3$ molecules to interior electrons and a constant surface charge is present. This molecule has the expected effect on the PL intensity and is unlike mobile electrons in dynamical behavior.

**4.2. Temperature Dependence of Electron Hopping through $TiO_2$ Particles.** An approximate estimate of the effect of temperature on hopping transport was obtained by measuring the discharge decay behavior of the charged $TiO_2$ surface at various temperatures. Figure 5 shows that, after charging to a near-maximum condition, the decay rate of the discharge process increases as temperature is increased in the range from 84 to 140 K. The Arrhenius plot of these data shows that the activation energy for the decay rate is 0.015 ± 0.008 eV. This activation energy relates to the barrier for particle-to-


dx.doi.org/10.1021/jp407765r | J. Phys. Chem. C 2013, 117, 24189−24195

particle transport of electrons, where activation energies of 0.030−0.100 eV have been found for such transport process in capped CdSe quantum dots and capped silver nanocrystals.[46,47] Our measurements cannot discriminate an activated process for transport from electron-trap-to-trap-site on the $TiO_2$ particle surfaces compared to electron hopping from $TiO_2$ particle to $TiO_2$ particle.

**4.3. Estimates of Electron Mobility in Hopping through $TiO_2$ Particles.** An approximate estimate can be made of the mobility of the electrons using the time constants for decay of charge and crude estimates for the diffusion lengths and electrostatic potential between the fully charged front face of the $TiO_2$ powder and the back face. For the fully charged $TiO_2$ surface in Figure 5, we measured a discharge rate constant at 140 K of $k = 4.6 \times 10^{-4}$ $s^{-1}$. Assuming that the electrical potential at the $TiO_2$ front surface is on the order of 0.1 V,[31,48] that the thickness of the powder layer is $9.5 \times 10^{-5}$ m, and that the dielectric constant of powdered $TiO_2$ is 100,[49] we estimate that the electric field across the depth of our $TiO_2$ sample is on the order of $10^3$ V $m^{-1}$. By extrapolation of the Arrhenius plot in Figure 5, we estimate that the 300 K electron mobility is $1 \times 10^{-10}$ $m^2$ $V^{-1}$ $s^{-1}$. This value is in satisfactory agreement with Nelson et al.'s value for electron mobility [$(1 \times 10^{-11})$−$(1 \times 10^{-10})$ $m^2$ $V^{-1}$ $s^{-1}$] in a porous $TiO_2$ network obtained under vacuum conditions by time-of-flight measurements at 300 K.[27]

## 5. SUMMARY OF RESULTS

The following results were obtained from this study of the production and decay of photoluminescence in a compressed $TiO_2$ powder of n-type material, working in high vacuum with relatively clean surfaces:

(1) Discharging rates have been measured as a function of temperature. It was found that $TiO_2$ powder, when charged by the surface photovoltage effect on its outer surface by exposure to UV light (3.88 eV), will discharge in the dark as electrons originally transported into the $TiO_2$ bulk are allowed to back-diffuse to the surface.

(2) The data obtained from cyclical experiments of charging and discharging indicate that the charge transport can be understood by simple considerations of the behavior of a planar slab of $TiO_2$ powder.

(3) The activation energy for the electron-transport process was measured to be 0.015 ± 0.008 eV in the 84−140 K temperature range.

(4) An estimate of the electron mobility of $1 \times 10^{-10}$ $m^2$ $V^{-1}$ $s^{-1}$ was made for the transport process and the process observed here is very slow compared to *in situ* electron transport processes in crystalline $TiO_2$. It is assigned to electron hopping either from $TiO_2$ surface site to surface site, or from nanocrystallite to nanocrystallite in the $TiO_2$ matrix.

(5) Although expected changes in PL intensity are achieved by adsorption of an immobile donor molecule, charge mobility effects in the $TiO_2$ are not seen as for mobile electrons.

## AUTHOR INFORMATION

### Corresponding Author

*E-mail: johnt@virginia.edu.

### Notes

The authors declare no competing financial interest.

## ACKNOWLEDGMENTS

We acknowledge with thanks the support of this work by the Army Research Office under Grant 55748CH, as well as a fellowship for Ana Stevanovic from AES Corp. through the AES Graduate Fellowships in Energy Research Program at the University of Virginia.

## REFERENCES

(1) Hagfeldt, A.; Gratzel, M. Light-Induced Redox Reactions in Nanocrystalline Systems. *Chem. Rev.* **1995**, *95*, 49−68.
(2) Law, M.; Greene, L. E.; Johnson, J. C.; Saykally, R.; Yang, P. D. Nanowire Dye-Sensitized Solar Cells. *Nat. Mater.* **2005**, *4*, 455−459.
(3) Kamat, P. V. $TiO_2$ Nanostructures: Recent Physical Chemistry Advances. *J. Phys. Chem. C* **2012**, *116*, 11849−11851.
(4) O'Regan, B.; Gratzel, M. A Low-Cost, High-Efficiency Solar Cell Based on Dye-Sentisized Collodial $TiO_2$ Films. *Nature* **1991**, *353*, 737−740.
(5) Bach, U.; Lupo, D.; Comte, P.; Moser, J. E.; Weissortel, F.; Salbeck, J.; Spreitzer, H.; Gratzel, M. Solid-State Dye-Sensitized Mesoporous $TiO_2$ Solar Cells with High Photon-to-Electron Conversion Efficiencies. *Nature* **1998**, *395*, 583−585.
(6) Gratzel, M. Photoelectrochemical Cells. *Nature* **2001**, *414*, 338−344.
(7) Linsebigler, A. L.; Lu, G. Q.; Yates, Jr., J. T. Photocatalysis on $TiO_2$ Surfaces: Principles, Mechanisms, and Selected Results. *Chem. Rev.* **1995**, *95*, 735−758.
(8) Mills, A.; LeHunte, S. An Overview of Semiconductor Photocatalysis. *J. Photochem. Photobiol. A: Chem..* **1997**, *108*, 1−35.
(9) Fujishima, A.; Zhang, X.; Tryk, D. A. $TiO_2$ Photocatalysis and Related Surface Phenomena. *Surf. Sci. Rep.* **2008**, *63*, 515−582.
(10) Thompson, T. L.; Yates, Jr., J. T. Surface Science Studies of the Photoactivation of $TiO_2$—New Photochemical Processes. *Chem. Rev.* **2006**, *106*, 4428−4453.
(11) Crossland, E. J. W.; Noel, N.; Sivaram, V.; Leijtens, T.; Alexander-Webber, J. A.; Snaith, H. J. Mesoporous $TiO_2$ Single Crystals Delivering Enhanced Mobility and Optoelectronic Device Performance. *Nature* **2013**, *495*, 215−219.
(12) Ducati, C. Materials Science Porosity in a Single Crystal. *Nature* **2013**, *495*, 180−181.
(13) Gratzel, M. Dye-Sensitized Solid-State Heterojunction Solar Cells. *MRS Bull.* **2005**, *30*, 23−27.
(14) Duzhko, V.; Timoshenko, V. Y.; Koch, F.; Dittrich, T. Photovoltage in Nanocrystalline Porous $TiO_2$. *Phys. Rev. B.* **2001**, *64*, 075204.
(15) Schroder, D. K. Surface Voltage and Surface Photovoltage: History, Theory and Applications. *Meas. Sci. Technol.* **2001**, *12*, R16−R31.
(16) Dittrich, T.; Weidmann, J.; Koch, F.; Uhlendorf, I.; Lauermann, I. Temperature- and Oxygen Partial Pressure-Dependent Electrical Conductivity in Nanoporous Rutile and Anatase. *Appl. Phys. Lett.* **1999**, *75*, 3980−3982.
(17) Forro, L.; Chauvet, O.; Emin, D.; Zuppiroli, L.; Berger, H.; Levy, F. High Mobility n-Type Charge Carriers in Large Single Crystals of Anatase ($TiO_2$). *J. Appl. Phys.* **1994**, *75*, 633−635.
(18) Yagi, E.; Hasiguti, R. R.; Aono, M. Electronic Conduction above 4 K of Slightly Reduced Oxygen-Deficient Rutile $TiO_{2-x}$. *Phys. Rev. B.* **1996**, *54*, 7945−7956.
(19) Benzaquen, R.; Benzaquen, M.; Charbonneau, S.; Poole, P. J.; Rao, T. S.; Lacelle, C.; Roth, A. P.; Leonelli, R. Evidence from Electrical Transport and Photoluminescence Spectroscopy of a Band of Localized Deep Donors in High-Purity *n*-Type InP Grown by Chemical-Beam Epitaxy. *Phys. Rev. B.* **1994**, *50*, 16964−16972.
(20) Nelson, J.; Chandler, R. E. Random Walk Models of Charge Transfer and Transport in Dye Sensitized Systems. *Coord. Chem. Rev.* **2004**, *248*, 1181−1194.
(21) Barzykin, A. V.; Tachiya, M. Mechanism of Charge Recombination in Dye-Sensitized Nanocrystalline Semiconductors: Random Flight Model. *J. Phys. Chem. B* **2002**, *106*, 4356−4363.

(22) Anta, J. A.; Nelson, J.; Quirke, N. Charge Transport Model for Disordered Materials: Application to Sensitized $TiO_2$. *Phys. Rev. B.* **2002**, 65.
(23) Eppler, A. A.; Ballard, I. N.; Nelson, J. Charge Transport in Porous Nanocrystalline Titanium Dioxide. *Phys. E* **2002**, *14*, 197−202.
(24) Cao, F.; Oskam, G.; Meyer, G. J.; Searson, P. C. Electron Transport in Porous Nanocrystalline $TiO_2$ Photoelectrochemical Cells. *J. Phys. Chem.* **1996**, *100*, 17021−17027.
(25) Hendry, E.; Koeberg, M.; O'Regan, B.; Bonn, M. Local Field Effects on Electron Transport in Nanostructured $TiO_2$ Revealed by Terahertz Spectroscopy. *Nano Lett.* **2006**, *6*, 755−759.
(26) Dittrich, T.; Lebedev, E. A.; Weidmann, J. Electron Drift Mobility in Porous $TiO_2$ (Anatase). *Phys. Status Solidi A* **1998**, *165*, R5−R6.
(27) Aduda, B. O.; Ravirajan, P.; Choy, K. L.; Nelson, J. Effect of Morphology on Electron Drift Mobility in Porous $TiO_2$. *Int. J. Photoenergy* **2004**, *6*, 141−147.
(28) Kopidakis, N.; Schiff, E. A.; Park, N. G.; van de Lagemaat, J.; Frank, A. J. Ambipolar Diffusion of Photocarriers in Electrolyte-Filled, Nanoporous $TiO_2$. *J. Phys. Chem. B* **2000**, *104*, 3930−3936.
(29) Solbrand, A.; Lindstrom, H.; Rensmo, H.; Hagfeldt, A.; Lindquist, S. E.; Sodergren, S. Electron Transport in the Nanostructured $TiO_2$−Electrolyte System Studied with Time-Resolved Photocurrents. *J. Phys. Chem. B* **1997**, *101*, 2514−2518.
(30) Muraoka, Y.; Takubo, N.; Hiroi, Z. Photoinduced Conductivity in Tin Dioxide Thin Films. *J. Appl. Phys.* **2009**, 105.
(31) Zhang, Z.; Yates, J. T., Jr. Band Bending in Semiconductors: Chemical and Physical Consequences at Surfaces and Interfaces. *Chem. Rev.* **2012**, *112*, 5520−5551.
(32) Stevanovic, A.; Buttner, M.; Zhang, Z.; Yates, J. T., Jr. Photoluminescence of $TiO_2$: Effect of UV Light and Adsorbed Molecules on Surface Band Structure. *J. Am. Chem. Soc.* **2012**, *134*, 324−332.
(33) Eagles, D. M. Polar Modes of Lattice Vibration and Polaron Coupling Constants in Rutile ($TiO_2$). *J. Phys. Chem. Solids* **1964**, *25*, 1243−1251.
(34) Cardona, M. H., G. Optical Properties and Band Structure of Wurtzite-Type Crystals and Rutile. *Phys. Rev. B.* **1964**, *137*, A1467.
(35) Ghosh, G. *Handbook of Optical Constants of Solids*; Academic Press: New York, 1985.
(36) Stevanovic, A.; Yates, J. T., Jr. Probe of $NH_3$ and CO Adsorption on the Very Outermost Surface of a Porous $TiO_2$ Adsorbent Using Photoluminescence Spectroscopy. *Langmuir* **2012**, *28*, 5652−5659.
(37) Kronik, L.; Shapira, Y. Surface Photovoltage Spectroscopy of Semiconductor Structures: At the Crossroads of Physics, Chemistry and Electrical Engineering. *Surf. Interface Anal.* **2001**, *31*, 954−965.
(38) Jing, L. Q.; Sun, X. J.; Shang, J.; Cai, W. M.; Xu, Z. L.; Du, Y. G.; Fu, H. G. Review of Surface Photovoltage Spectra of Nano-Sized Semiconductor and Its Applications in Heterogeneous Photocatalysis. *Sol. Energy Mater. Sol. Cells* **2003**, *79*, 133−151.
(39) Lantz, J. M.; Corn, R. M. Electrostatic Field Measurements and Band Flattening During Electron-Transfer Processes at Single-Crystal $TiO_2$ Electrodes by Electric-Field-Induced Optical Second Harmonic Generation. *J. Phys. Chem.* **1994**, *98*, 4899−4905.
(40) Hollingsworth, R. E.; Sites, J. R. Photoluminescence Dead Layer in p-Type InP. *J. Appl. Phys.* **1982**, *53*, 5357−5358.
(41) Ando, K.; Yamamoto, A.; Yamaguchi, M. Surface Band Bending Effects on Photoluminescence Intensity in n-InP Schottky and MIS Diodes. *Jpn. J. Appl. Phys.* **1981**, *20*, 1107−1112.
(42) King, D. A.; Madey, T. E.; Yates, Jr., J. T. Interaction of Oxygen with Polycrystalline Tungsten. II. Corrosive Oxidation. *J. Chem. Phys.* **1971**, *55*, 3247−3253.
(43) Berger, T.; Sterrer, M.; Diwald, O.; Knozinger, E.; Panayotov, D.; Thompson, T. L.; Yates, Jr., J. T. Light-Induced Charge Separation in Anatase $TiO_2$ Particles. *J. Phys. Chem. B* **2005**, *109*, 6061−6068.
(44) Ke, S. C.; Wang, T. C.; Wong, M. S.; Gopal, N. O. Low Temperature Kinetics and Energetics of the Electron and Hole Traps in Irradiated $TiO_2$ Nanoparticles as Revealed by EPR Spectroscopy. *J. Phys. Chem. B* **2006**, *110*, 11628−11634.
(45) Szczepankiewicz, S. H.; Moss, J. A.; Hoffmann, M. R. Slow Surface Charge Trapping Kinetics on Irradiated $TiO_2$. *J. Phys. Chem. B* **2002**, *106*, 2922−2927.
(46) Yu, D.; Wang, C. J.; Wehrenberg, B. L.; Guyot-Sionnest, P. Variable Range Hopping Conduction in Semiconductor Nanocrystal Solids. *Phys. Rev. Lett.* **2004**, 92.
(47) Doty, R. C.; Yu, H. B.; Shih, C. K.; Korgel, B. A. Temperature-Dependent Electron Transport through Silver Nanocrystal Superlattices. *J. Phys. Chem. B* **2001**, *105*, 8291−8296.
(48) Rothschild, A.; Komem, Y.; Levakov, A.; Ashkenasy, N.; Shapira, Y. Electronic and Transport Properties of Reduced and Oxidized Nanocrystalline $TiO_2$ Films. *Appl. Phys. Lett.* **2003**, *82*, 574−576.
(49) Parker, R. A. Static Dielectric Constant of Rutile ($TiO_2$), 1.6−1060 K. *Phys. Rev. B* **1961**, *124*, 1719−1722.
(50) Ohno, T.; Sarukawa, K.; Tokieda, K. Morphology of a $Tio_2$ Photocatalyst (Degussa, P-25) Consisting of Anatase and Rutile Crystalline Phases. *J. Catal.* **2001**, *203*, 82−86.